International Forum on Aeroelasticity and Structural Dynamics
IFASD 2024
17-21 June 2024, The Hague, The Netherlands

# CONTRIBUTION OF THE GROUND VIBRATION TESTS FOR THE PREPARATION OF FLUTTER SUPPRESSION FLIGHT TEST CAMPAIGNS: CASE OF THE FLIPASED P-FLEX UAV

**Nicolas. Guérin[1], Cyrille. Stephan[1], Pascal. Lubrina[1], Keith. Soal[2], Martin. Tang[2], Robin. Volkmar[2], Yves. Govers[2], Thiemo. Kier[3], Julius. Bartasevicius[4], Daniel. Teubl[4], Szabolcs. Toth[5], Bálint. Vanek[5]**

[1]ONERA – The French Aerospace Lab, Université Paris Saclay
Aerodynamics Aeroelasticity Acoustics Department
Experimental Aeroelasticity and Structural Dynamics Group
29 avenue de la division Leclerc, F-92322 Châtillon, France
nicolas.guerin@onera.fr

[2]German Aerospace Center (DLR)
Institute of Aeroelasticity
Structural Dynamics and System Identification
Bunsenstraße 10, 37073 Göttingen, Germany

[3]German Aerospace Center (DLR)
Institute of System Dynamics and Control
Aircraft Systems Dynamics
Münchner Straße 20, 82234 Oberpfaffenhofen-Wessling, Germany

[4]Technical University of Munich
Institute of Aircraft Design
Boltzmannstrasse 15, 85748 Garching b. Munich, Germany

[5]Institute for Computer Science and Control (SZTAKI)
Systems and Control Lab
Kende u. 13-17, 1111 Budapest, Hungary

**Keywords:** Ground Vibration Test, Active Flutter Suppression, FliPASED

**Abstract:** With the everlasting reach for lighter and more fuel-efficient aircraft structures, aircraft designs become more and more flexible. This leads to both increased deformation of the airframe under aerodynamic load, as well as more coupling between the structural static and dynamic behaviour and the surrounding airflow, potentially leading to the dreaded phenomenon of flutter. This dangerous behaviour has limited potential aircraft design optimization, hence impaired carbon footprint reduction. In order to circumvent this constraint, active flutter suppression through fast actuators and control surfaces was investigated during the FLEXOP and subsequent FliPASED projects, on a research high aspect ratio fixed wing UAV. Such control strategies, though of great interest thanks to their capability to control a wide variety of behaviour, also come with great risks if badly designed. They must therefore be conceived with very good knowledge of the controlled structure, as well as properly verified through an extensive test phase.

This paper focuses on the identification of the structural dynamic behaviour of the FliPASED P-FLEX UAV during a Ground Vibration Test (GVT) campaign. The paper presents the GVT organization, from instrumentation to analysis, including test configurations accounting for high-bandwidth actuators as well as devices, designed to help increase or decrease the flutter coupling, so-called flutter stoppers.

The paper describes the structural dynamic behaviour of the P-FLEX UAV and the influence of the different mechanical components on this behaviour. Due to multiple specific features of this aircraft including high aspect ratio and custom designed high-bandwidth actuators, this GVT proved difficult to achieve for both organizational and technical reasons. The paper presents the main problems associated with these specific features.

Although the P-FLEX UAV is of a peculiar design with respect to commercial aircraft, the observations made on this aircraft will be of great interest for future civilian aircraft designs that tend towards very high aspect ratio wings equipped with numerous active flutter suppression control surfaces.

## 1 INTRODUCTION

The FliPASED project [1] — successor of the FLEXOP project [2] — was dedicated to the design of an *Unmanned Aerial Vehicle* (UAV) capable of *Active Flutter Suppression* (AFS). The project team, led by the Hungarian institute for computer science and control (SZTAKI), and composed of the Technical University of Munich (TUM), the German aerospace centre (DLR) and the French aerospace lab (ONERA), worked on the numerous technical challenges that needed overcoming to achieve an in-flight demonstration of such a capacity.

In fact, though such a UAV is much easier to design than a fully certified aircraft, demonstrating the effectiveness of an AFS control system required the design and manufacturing of an aircraft that was prone to flutter — yet safe to operate — with wideband actuators, controllers, and sensors.

As is usually done for larger manned aircraft, the FliPASED UAV was submitted to a *Ground Vibration Test* (GVT) to estimate its natural dynamic behaviour, in order to update the structural dynamic model of the aircraft, the control laws, as well as the flutter predictions performed during the initial design phase. This ground vibration test was conducted by a joint team of ONERA and DLR personnel, and was performed at the DLR institute of Aeroelasticity in Göttingen. This test also involved personnel from TUM who handled the aircraft structure and base systems, along with people from SZTAKI and DLR Oberpfaffenhofen that worked on controller and model updating.

The campaign spanned two weeks, focused on a main structural, flutter-prone, configuration of the aircraft, as well as two complimentary configurations that proved to be flutter-free. Overall, the campaign led to the realization of about 80 measurement runs, and 41 modes were delivered out of 439 identifications.

This paper presents the aircraft, the GVT organization and main results as well as hopefully helpful observations made during this GVT for further similar projects e.g. CONCERTO [3] or TU-FLEX [4].

## 2 AIRCRAFT DESCRIPTION

The FliPASED p-FLEX UAV — visible in figure 1 — is a 70 kg aircraft of tube and wing design, fitted with one dorsal microturbine engine, main underbelly landing gear and a V-tail. The fuselage is 3.4 m long, its centre part contains most of the systems of the aircraft, as shown

(a) FliPASED P-FLEX UAV in flight © DLR [5].

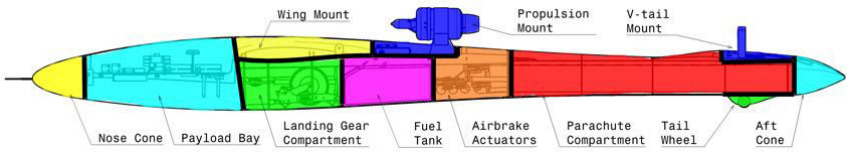


(b) Aircraft systems layout (reproduced from [6, Fig. 20])

Figure 1: FliPASED P-FLEX UAV.

in figure 1b, including the fuel tank and further front, the onboard computer and power systems. The nose is fitted with an anemometric boom. The aft part is equipped with two air brakes, that were locked during the GVT, and an emergency parachute. The UAV has a wingspan of 7 m, and an aspect ratio of roughly 20 with an 18° sweep angle. Each wing is fitted with 4 control surfaces. The outer ailerons are actuated with wideband so-called DirectDrive actuators, and participate in the AFS control system. Moreover, an appendage was mounted on both wings, a so-called *flutter-stopper*. These components are composed of a *Carbon Fibre Reinforced Plastic* (CFRP) hollow beam mounted on a relatively stiff CFRP support under the wing at about 70 % of the wingspan and fitted with a movable prismatic steel mass. They are dedicated to the (de-)stabilization of the aircraft flutter behaviour by means of inertia-axis displacement. For an in-depth presentation of the aircraft measurement and control systems, the reader is invited to refer to [7].

## 3 GVT ORGANIZATION

### 3.1 Objectives

Although a GVT was performed on the earlier model of this aircraft — the T-FLEX — demonstrator [8], this aircraft was unfortunately lost during a flight test in 2022. The crash was followed by a rebuild of the UAV, which was fitted with a new wing set, to demonstrate the AFS in flight. It was therefore mandatory to verify the aircraft before flutter tests, and to update the models involved in the AFS control.

### 3.2 Teams and roles

The GVT of the FliPASED aircraft was conducted by a team from ONERA and DLR at the DLR Institute of Aeroelasticity in Göttingen, for both interoperability training and research purposes. A joint test team gathered around the aircraft as depicted in figure 2. The team was composed of

measurement and mechanical operators, engineers and computer scientists for data acquisition, signal processing, modal analysis and modal model correlation and a campaign leader to ensure high quality results.

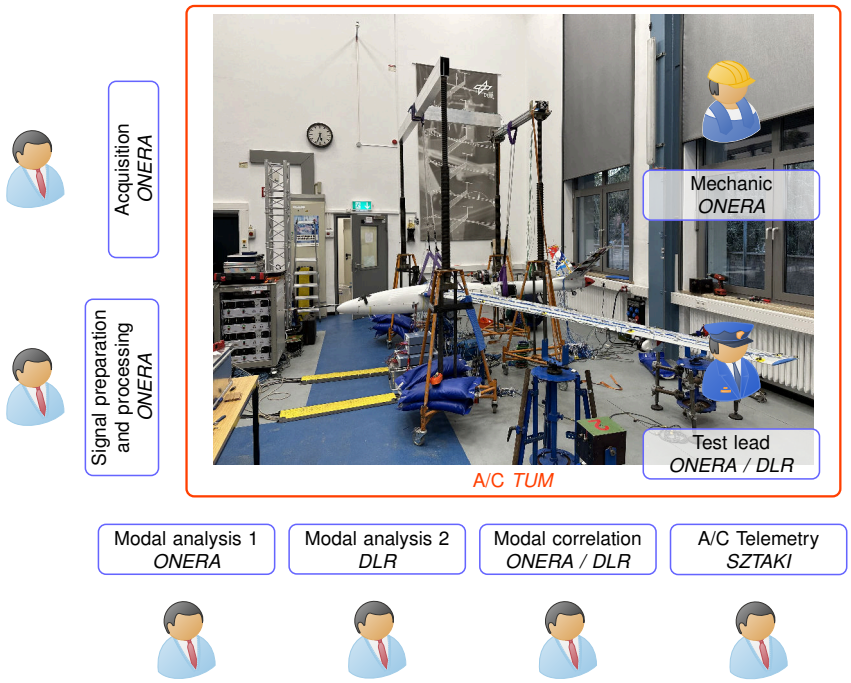


Figure 2: Test setup overview.

### 3.3 Mechanical configurations and boundary conditions

The aircraft was suspended to a mechanical frame using soft bungee chords as shown in figure 2 in order to separate the elastic modes from the rigid body modes. These bungees were positioned close to the fuselage under the wing root on each side, and under a fuselage frame, aft of the engine. In order to minimize slippage from their initial position and reduce the risk of damage to the aircraft, foam sheets were placed between the aircraft surfaces and the bungees, which were then taped to the aircraft surface.

During the test, the aircraft weighed 70 kg which included 10 kg of fuel load. During measurements, the canopy was closed, and additional masses were fitted onto the airframe in order to account for missing components that would be present during the flight test campaign, but that could either not be available or compatible with the GVT operations. At the beginning of the GVT campaign, all aircraft systems were powered on and flight ready. However, large electromagnetic noise levels were quickly encountered, and the problem was rooted to the DirectDrive actuators linked with the AFS-capable control surfaces, the outer ailerons. Therefore, the majority of the campaign was performed with aileron actuators unpowered. This electromagnetic compatibility problem, which could have posed many problems with regard to the project objectives, is further discussed in section 4.7.

Three structural configurations were tested during this GVT campaign

- C1a : aircraft with flutter stopper masses in aft position (flutter-prone design point). This is the main configuration that was tested
- C1b : aircraft with flutter stopper masses in forward position (flutter-free design point). Three excitation runs were performed, all on the wings

- C1d : aircraft with flutter stopper rods removed. This configuration was not initially planned. It was performed as a fast verification point for the test instrumentation with a simpler aircraft structure.

The aircraft was suspended using three bungees and slings, two fitted on the wing roots on each side of the fuselage, and one under the fuselage close to a fuselage web location. The suspension was equipped with triaxial accelerometers, to avoid any miss interpretation between the suspension chord modes and the aircraft flexible modes. The suspension gantry was equipped with accelerometers as well, for monitoring purposes, and weighted to ensure its stability.

### 3.4 Instrumentation

The aircraft was instrumented with a mix of equipment from DLR and ONERA, totalling about 150 IEPE accelerometers, Siemens SCADAS Lab and SCADAS Mobile acquisition frontends, PRODERA power amplifiers and PRODERA and ONERA electrodynamic shakers. SZTAKI provided a ground control station with telemetry capabilities to control the aircraft state and record data using internal sensors for other partners.

Figure 3 depicts the measurement locations and directions. Given the relatively low weight of

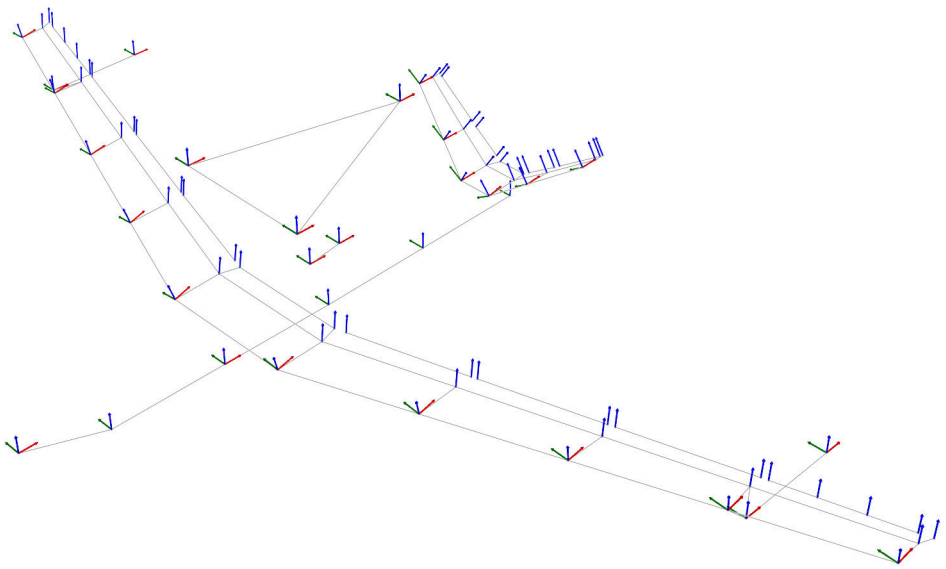

Figure 3: Aircraft sensor locations and directions. Local X (→), Y (→), Z (→) sensor directions.

the aircraft, mostly very light sensors were installed, although slightly larger triaxial sensors were used as well. These were specially fitted to the leading edge of lifting surfaces, the engine, the anemometric boom, and the flutter-stopper devices. The list of sensors and nomenclature used is detailed in table 1a. The suspension bungees and supporting structure — though its sensors are not represented or listed here — were instrumented as well, which proved useful during the correlation of the modal data. The only massive component that was not instrumented is the landing gear which was considered relatively stiff. All sensors were positioned tangentially to the local surface, explaining the various directions observed in figure 3. Dedicated triaxial sensors were positioned at two locations on the flutter stopper beams, as shown in figure 4.

5 excitation points were used throughout the campaign, these are listed in table 1b and shown in figure 5. Two excitation sites were exploited on the wing in order to best identify the 2 and 3 node wing bending modes. All excitation points were glued onto the aircraft structure,

Table 1: List of the instrumentation used during the GVT.

(a) List of sensors per aircraft structural components. Left/Right (L/R) sensor counts must be doubled to account for all sensors.

| Component | Sensors |
|---|---|
| L/R Wing | 6 XYZ + 7 Z |
| L/R Aileron 1 | 2 Z |
| L/R Aileron 2 | 2 Z |
| L/R Aileron 3 | 2 Z |
| L/R Aileron 4 | 4 Z |
| L/R Direct Drive | 1 XYZ |
| L/R Stabilizer | 3 XYZ + 5Z |
| L/R Elevator 1 | 2 Z |
| L/R Elevator 2 | 2 Z |
| Fuselage | 1 XYZ + 4YZ |
| Engine | 2 XYZ |
| Nose Boom | 1 XYZ |
| Driving Points | 2 X + 1Y + 3 Z |
| Suspension Device | 3 XYZ |

(b) List of excitation points used during the GVT. Each excitation point is equipped with a force cell as well as a dedicated accelerometer.

| Component | Directions |
|---|---|
| L/R Inner Wing | X, Z |
| L/R Outer Wing Z | Z |
| Fuselage | Y, Z |

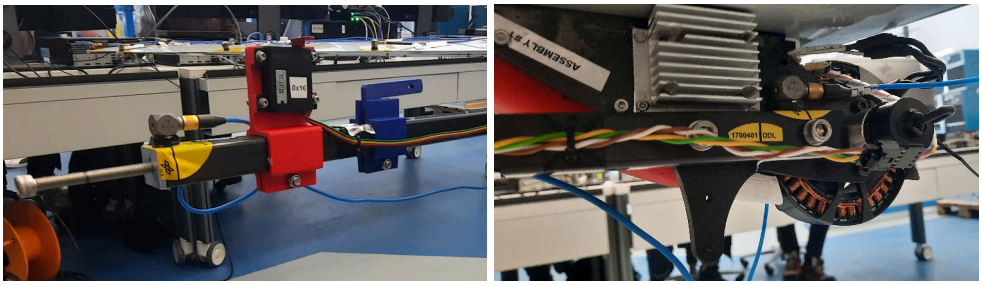

(a) Aft sensor. (b) Front sensor.

Figure 4: Flutter stopper sensors.

(a) Fuselage Y. (b) Fuselage Z. (c) Inner Wing Z. (d) Inner Wing X.

Figure 5: Excitation points, equipped with a 47 N ONERA shaker along with its sensing elements.

via interface parts. The wing X excitation points were glued through 3D-printed conformal interface parts.

Given the amount of sensors fitted inside the aircraft for the AFS control system, a synchroniza-

tion of the *Flight Test Instrumentation* (FTI) and GVT instrumentation was attempted. Although this problematic is generally trivial on modern acquisition systems, e.g. by means of IRIG-clock synchronization [9], the on-board computer — based on a Raspberry Pi — was not designed for this which made it impossible to synchronize both acquisition systems that way. In order to circumvent this problem, a synchronization signal was generated by the SCADAS during GVT operations. This signal was subsequently acquired through a 3.3 V input on the aircraft computer, as well as a SCADAS analogue input. The synchronization signal was a random white noise signal, that would undoubtedly suffer from delays between the two systems. The synchronization processing and results are discussed in section 4.5.

### 3.5 Methodology

Most analyses were performed using the *Phase Separation Method* (PSM) under random or swept sine excitations, using the PolyMAX identification software [10] along with dedicated in house software from DLR and ONERA teams [11].

## 4 RESULTS

### 4.1 Modal content

The modal content of the main configuration (C1a) is listed in table 2. Although dynamic behaviour could be observed above 33 Hz, no modal extraction could be performed with sufficient accuracy above that frequency.

Table 2: Modal property tables for FliPASED configuration C1a.

| No. | Name | Damped Freq. [Hz] | Damping [%] | Gen. Mass [kg.m$^2$] |
|---|---|---|---|---|
| 1 | ac_y_trans-S | 0.867 | 0.83 | 284.99 |
| 2 | ac_pitch-S | 0.888 | 5.14 | 12.57 |
| 3 | ac_x_trans-S | 1.009 | 1.69 | 72.83 |
| 4 | ac_z_trans-S | 1.143 | 4.61 | 22.77 |
| 5 | ac_yaw-A | 1.797 | 0.77 | 44.86 |
| 6 | 2n_wing_bend-s | 2.938 | 1.10 | 5.08 |
| 7 | 3n_wing_bend-a | 7.220 | 0.79 | 3.24 |
| 8 | 1n_wing_inplane-a | 8.491 | 1.83 | 32.43 |
| 9 | wing_tors-s | 10.744 | 0.95 | 0.65 |
| 10 | wing_tors-a | 11.155 | 1.07 | 0.69 |
| 11 | 4n_bending-s | 12.023 | 0.72 | 3.12 |
| 12 | vtail_rock-a | 12.501 | 3.36 | 0.64 |
| 13 | 2n_wing_inplane-s | 14.846 | 1.19 | 2.34 |
| 14 | flutterstop_right_y | 16.702 | 2.97 | 0.44 |
| 15 | mass_lat-a | 18.617 | 1.08 | 1.83 |
| 16 | mass_lat-s | 19.298 | 1.41 | 6.85 |
| 17 | 5n_wing_bend-a | 20.383 | 1.78 | 1.57 |
| 18 | flutterstop_left_y | 22.213 | 4.01 | 0.47 |
| 19 | 2n_fus_vert-s | 23.986 | 1.25 | 1.21 |
| 20 | 6n_wing_bend-s | 25.860 | 1.82 | 0.97 |
| 21 | 2n_fus_lat-a | 26.266 | 1.42 | 1.76 |
| 22 | 2n_tail_bend-s | 27.218 | 0.90 | 1.18 |
| 23 | 7n_wing_bend-A | 29.431 | 1.37 | 2.09 |
| 24 | 2n_tail_bend-s? | 29.466 | 1.10 | 1.40 |
| 25 | engine_x-s | 32.172 | 0.74 | 2.86 |
| 26 | 7n_wing_bend-A??? | 32.864 | 1.15 | 0.92 |
| 27 | 2nd_wing_tors-a | 33.350 | 3.45 | 0.74 |

### 4.2 Rigid body properties

Rigid body modes of the aircraft identified during this campaign were not extensively identified. While the frequency and damping factors may be well identified, the generalized masses for these modes must be taken with caution. This can be explained by the usage of lightweight sensors during this GVT to reduce perturbation of the aircraft structural behaviour by the additional sensor masses. In fact, these sensors show poor sensitivity at low frequencies for technological reasons, leading to ill-identified generalized masses. Finally, the rigid body roll mode could not be identified during the modal analysis, due to its very low frequency.

### 4.3 Comparison between mechanical configurations

Since the flutter stopper systems were designed to ensure the aircraft safety, before attempting flutter flight tests, ensuring the effectiveness of their design was of utmost importance.

A list of common mode shapes identified in the three structural configurations mentioned in 3.3 was assembled and their frequency and damping properties were compared. As a recall, only configuration C1a was extensively analysed, and in C1b and C1d only wing excitations were performed.

Figure 6 depicts the qualitative ordering of modal families in each configuration. Quite un-

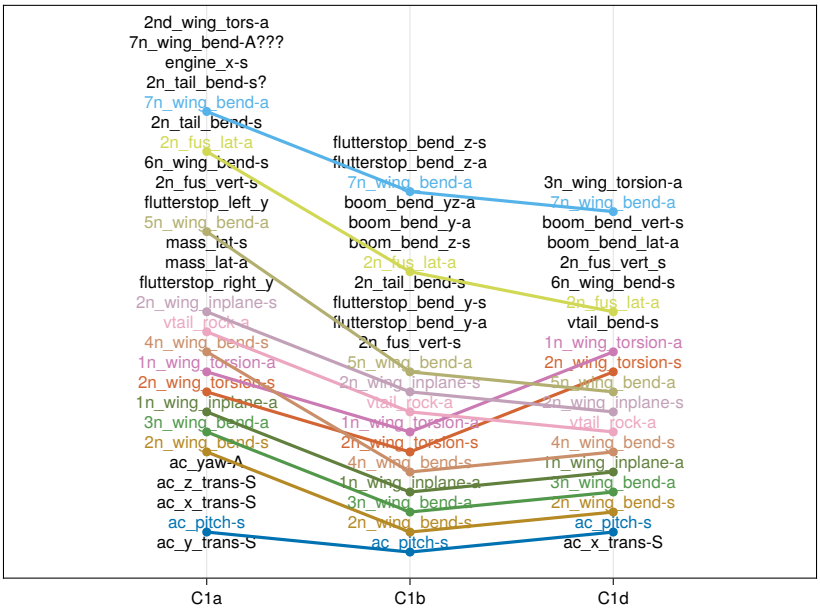


Figure 6: Frequency organization of modal families identified in C1a, C1b and C1d.

derstandably, some modes identified during C1a excitations were *missed* in C1b and C1d due to the reduced measurements for these two configurations, especially rigid body motions and higher frequency modes. Nevertheless, the qualitative effect of the flutter stopper devices on the wing torsion modes can be highlighted here. Indeed, in C1b — flutter stopper masses moved in forward position, closer to the torsion line — the first symmetric and antisymmetric torsions shift above the 4 node wing bending mode, and their shape visible in figure 7 change radically, as they were initially dominated by the flutter stopper motion. In the same conditions, bending modes seem to be very little impacted, as designed, by the mass position modification. In C1d — flutter stopper removed — torsion modes are pushed even further up increasing separation with the first bending modes.

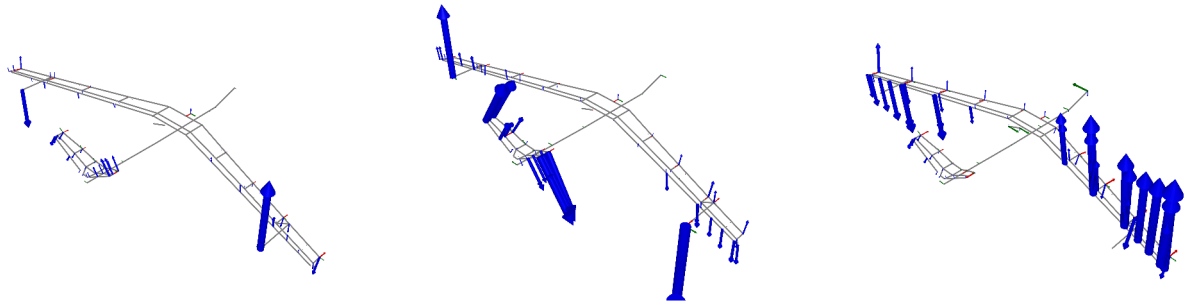

(a) 1st antisymmetric torsion

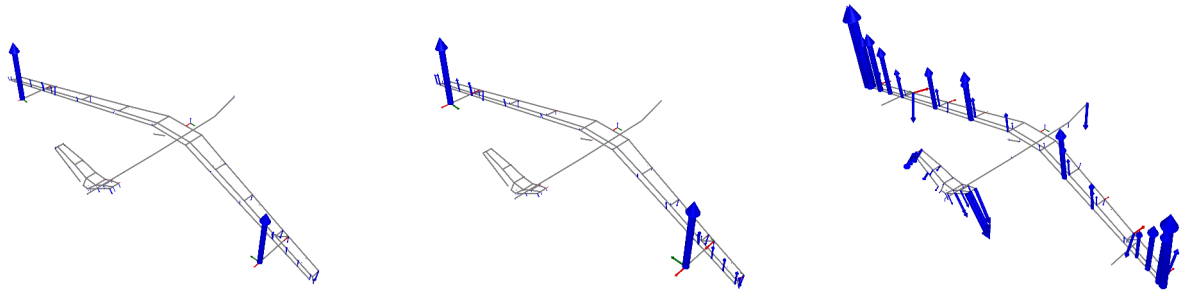

(b) 1st symmetric torsion

Figure 7: Comparison of the real part of modeshapes identified in C1a (left), C1b (middle) and C1d (right).

A quantitative comparison of modal frequencies (respectively dampings) is performed in figure 8 (respectively figure 9). A clear trend can be observed in terms of frequencies, where

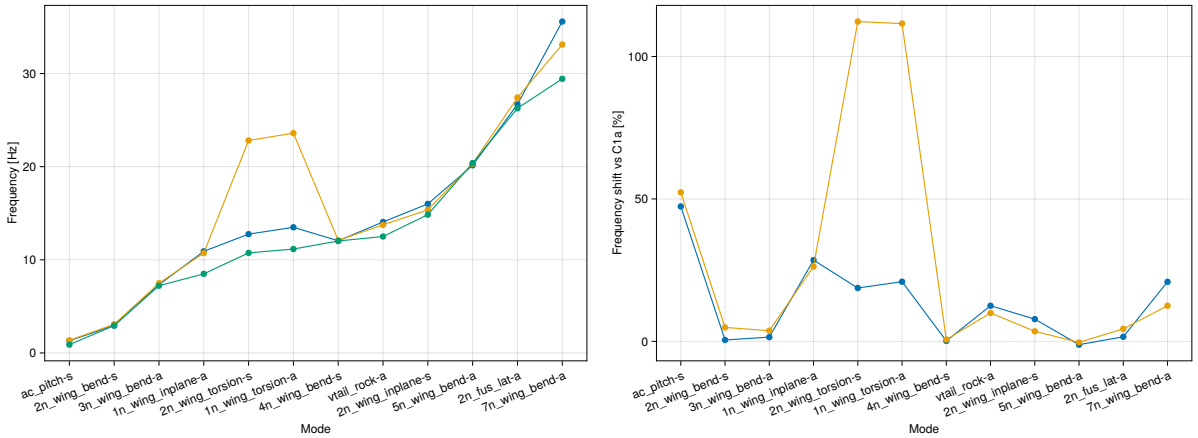


(a) Absolute values

(b) Relative shift w.r.t C1a.

Figure 8: Comparison of frequency properties of common modes identified in C1a (●●●), C1b (●●●) and C1d (●●●).

almost only the first torsion modes are influenced by the position, or even the presence, of the flutter stopper devices.

Two other types of behaviour can be highlighted. First, the pitch mode is also influenced by the flutter stopper condition, given the inertia modification due to the mass positions. Second, the so-called scissor mode — the first antisymmetric in-plane bending — is also influenced by the mass positions. This behaviour can be explained by the contribution of torsion in the in-plane motion, as visible in figure 10. There is also a much larger effect of the flutter stopper

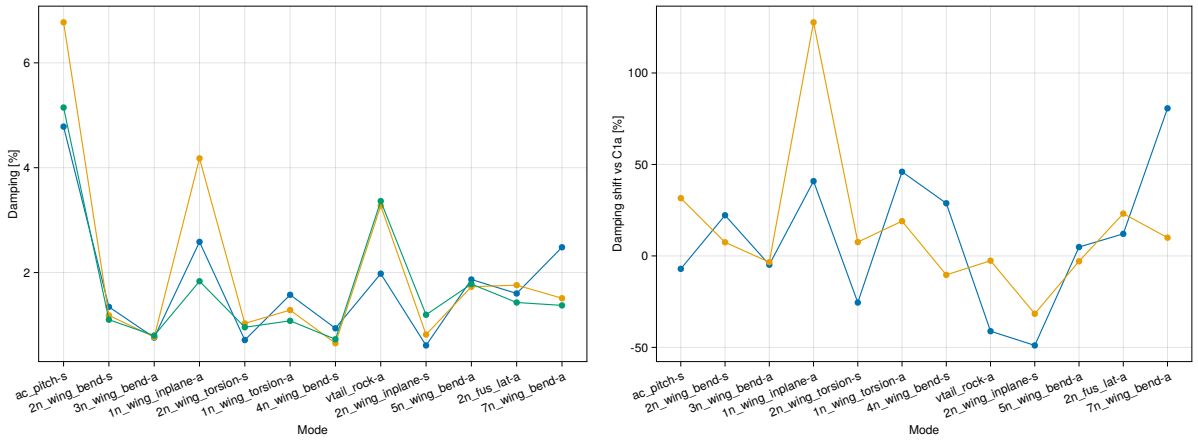


(a) Absolute values

(b) Relative shift w.r.t C1a.

Figure 9: Comparison of damping properties of common modes identified in C1a (●●●), C1b (●●●) and C1d (●●●).

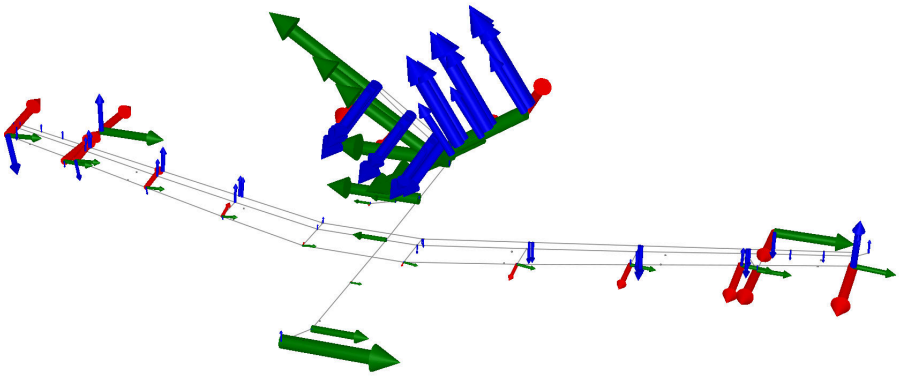

Figure 10: Real part of the scissor mode modeshape in C1a.

removal than that of the flutter stopper mass position, meaning that the flutter stopper design, might be optimized to reduce the mass of the flutter stopper device to obtain a better flutter mass weight/flutter stopper weight.

In terms of damping, there is no obvious influence worth commenting, except for the scissor mode, which shows quite a large variation between configurations, due to its overall nonlinear behaviour as discussed below.

### 4.4 Nonlinear behaviour

Some flexible mode suffers from poor identification, in particular, the one of mode No.12 (flutter stopper bending) identified in C1b. While there is no obvious clue as to why this mode suffers from poor identification, the fact that it is a flutter stopper mode could indicate and influence of the flutter mass inside the flutter stopper rod. In fact there is some free play between the mass and the rod, resulting in friction and impacts.

As a final comment, the frequency, and therefore the damping and modal masses of a few modes, in particular the in-plane bending mode, was without surprise difficult to ascertain. This particular mode stems from the flexibility of the linkage between the aircraft fuselage and wings. On this aircraft, this linkage is bolted. Such configurations are often prone to non-linear behaviour due to the high sensitivity of local sliding or even separation between initially in contact compo-

nents. This leads to complex structural behaviour on which linear modal identification reaches its limits. This is generally true for most linkage related movements. As an example, figure 11 displays the frequency response functions of the wing X direction accelerometers, in C1a, during three fuselage Y excitation runs at increasing excitation force levels. By compar-

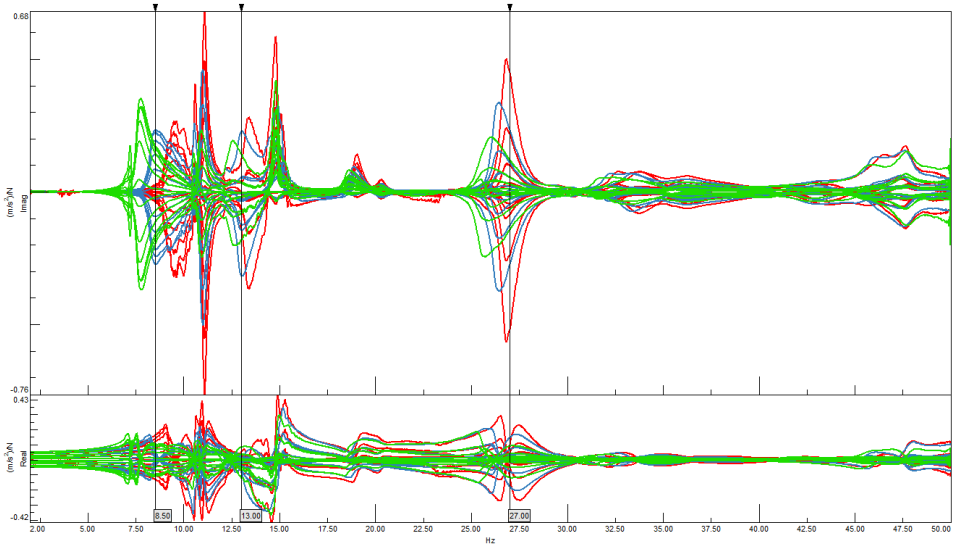


Figure 11: Frequency response functions of wing X direction accelerometer responses under fuselage Y excitation. Force voltage 0.25 V (—), 0.5 V (—), 1 V (—).

ing the frequency response function trends around 8.5 Hz, 13 Hz and 27 Hz, one can observe a frequency shift of the response amplifications towards lower frequencies, as well as variation of these amplifications. These observations are easily attributed to sliding phenomena in the aircraft structure. Given the identified modal data in table 2, one can link these nonlinear behaviour with the scissors/in-plane mode (mode shape in figure 10), the V-tail rock mode (mode shape in figure 12a) and the first lateral fuselage bending (mode shape in figure 12b).

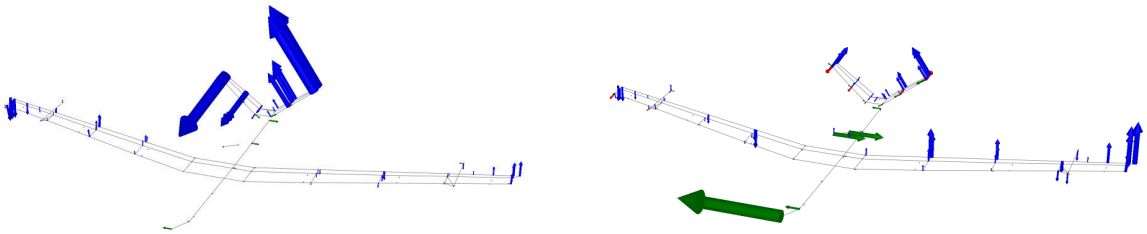

(a) V-tail rock mode. (b) First fuselage Y direction bending mode.

Figure 12: Real part of modeshapes identified in C1a.

### 4.5 GVT-FTI combination

As explained in section 3.4 a random signal was recorded by both the GVT acquisition system, as well as the aircraft FTI. The acquisition systems were configured such that the FTI signal was always longer that the GVT signal. These signals were subsequently compared to try and estimate the time delay between recorded data on both systems, both set to the same sampling frequency of 200 Hz. The delay estimation was based on the computation of the cross correlation between the two signals. The initial re-synchronization strategy assumed a constant lag between the two systems, due to the acquisition and processing chains. However, this proved ill-assumed and large phase shifts between the two signals remained, even after lag correction.

Indeed, the phase lag was actually varying during a measurement run as shown in figure 13. This result could be obtained by computing the cross correlation between windows of 300 sam-

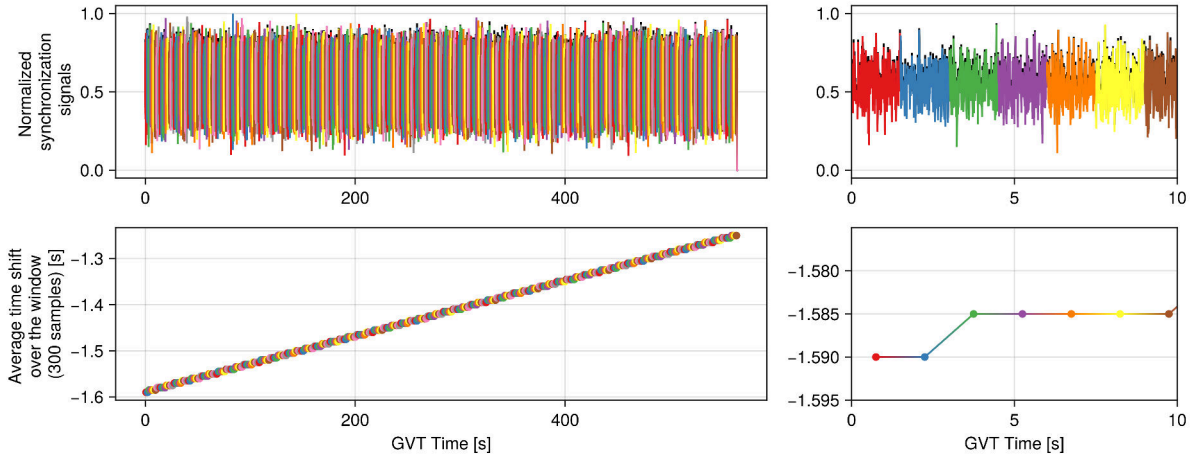


Figure 13: Illustration of the lag estimation between the GVT (—) and FTI (—)... (—) windows of the synchronization signals.

ples of the FTI-recorded signal vs the GVT signal. The lower left plot shows that the average time lag on a window variates from −1.59 s to −1.25 s over the full run, which means that an estimate of 68 samples were *lost* on the FTI with a rate of about 0.1205 S/s. Given that both the SCADAS and Raspberry Pi use crystal based clocks, with the SCADAS clock being calibrated with an error of less than ±40 ppm (or 0.008 Hz at 200 Hz), it seems unlikely that the variable lag comes from the acquisition systems themselves. Indeed, with such clock errors, over the course of a 564 s long run, and assuming the worst case scenario of opposite errors — one clock oversampling of 40 ppm the other undersampling, while the SCADAS error was measured at about 3 ppm — only about 10 samples may be lost. This increasing lag may however come from the non-deterministic sampling of the data due to CPU-loads on the Raspberry Pi later in the onboard processing chain. This could however not be investigated further, but it remains an important observation in case of long-term processing of signals on such demonstrators. It must be reminded that this system was initially not designed for modal analysis.

Rephased signals were subsequently analysed and *Frequency Response Functions* could be estimated between the GVT (accelerometer) and FTI (accelerometers and gyroscopes) sensors, and the GVT excitation forces as depicted in figure 14. The FRFs where further processed by means of polyreference frequency domain modal analysis comparable to [10]. Figure 14 also depicts poles obtained from such analyses based on the FTI accelerometer data, GVT accelerometer data and FTI gyroscope data. Despite the overall less noisy data from the GVT sensors, that lead to a clearer diagram, the stabilization diagrams show good agreement, especially in the frequency domain of the torsion modes ≈10 Hz where the AFS system should operate safely. Although such GVT/FTI common processing was only performed recently on a limited amount of data, such correlation between on-board and ground measurements could help calibrate AFS measurements systems to ensure good observability during flutter flight tests.

### 4.6 Flutter simulations

Based on the aforementioned GVT results, a complete review and update of the structural models available was performed, and multiple flutter simulations using the *Doublet Lattice Method* (DLM) [12] were performed by different partners. In particular, DLR performed a model up-

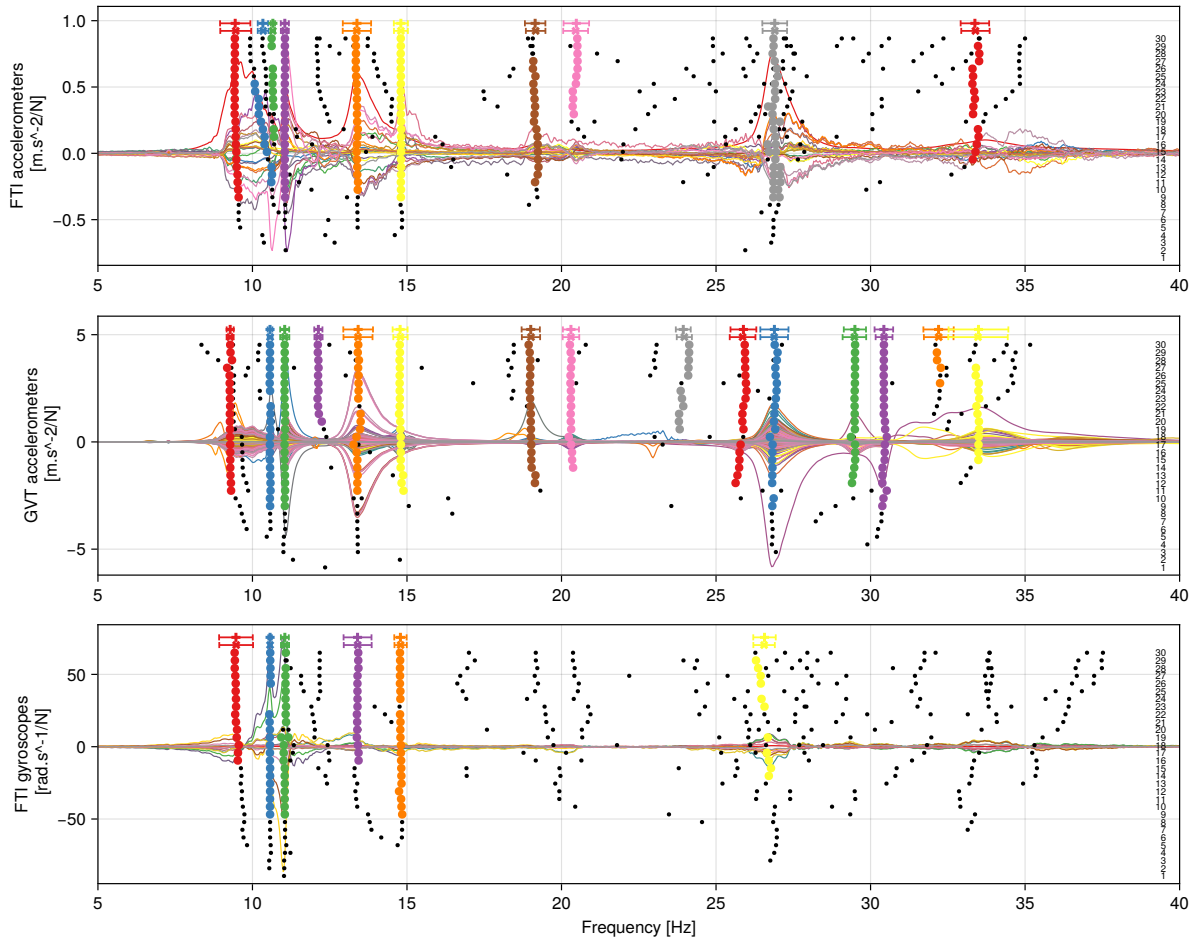


Figure 14: Stabilization diagrams obtained after frequency estimation over the lag-corrected signals between GVT and FTI sensors and GVT excitation forces during Run 15. Imaginary part of FRFs (—)... (—). Poles obtained from a polyreference modal analysis up to order 30 ( ● ). Clustered poles ( ● )... ( ● ). Average / Median pole over the cluster ( + ) / ( × ). −3 dB band around the cluster (⊢⊣).

dating of the stiffness and damping matrices of the structural dynamic model of the aircraft to perform flutter simulations with the $p$ and $p-k$ [13] methods. The simulations performed by DLR are further discussed in [14]. ONERA performed simulations using the $p-k$ [13] method using directly the experimental modes identified during the GVT. Although these particular simulations disregarded the effect of the AFS system, the results were very similar in terms of flutter speed to the ones obtained by the DLR.

All in all, these new simulations returned a very interesting result: the flutter mechanism to expect of this aircraft had changed. Indeed, while an antisymmetric behaviour was expected initially, this behaviour was pushed further up the flight domain, only for the symmetric wing–torsion coupling to reach flutter onset at about 55 m/s to 56 m/s instead of the initially estimated 50 m/s. As observed in [15], the initial finite element model of the FliPASED aircraft did not account for the in-plane bending (or scissor) mode, which could easily explain the change of flutter mechanism since this mode also possess a noticeable out-of-plane torsion-like contribution.

### 4.7 Lessons learned

While this GVT in itself was not of an extreme complexity, some lessons have been learned in terms of testing both very light and active structures.

Testing light structures is relatively complex on its own. In fact, these structures are easily influenced by the surrounding measurement or excitation instrumentation. The use of very light sensors, in order to reduce the intrusiveness of the sensor masses led to instrument the aircraft with non-TEDS sensors. This subsequently led to the late detection of instrumentation mis-cabling. It could prove interesting to possess a TEDS capability for very light sensors.

Due to the expected high aspect ratio of this aircraft and its various peculiarities, the test team expected the aircraft to show unconventional structural behaviour. This expectation bias led to some identification errors, that were in fact related to instrumentation issues. Moreover, due to the time constraints left for the GVT and the flight tests after the rebuild of the aircraft, and despite the research purpose of this project, the two weeks dedicated to this campaign were eventually not sufficient to fully test this aircraft. This is part is due to the intrinsic technical complexity of the aircraft, as well as the GVT itself. In fact, some aircraft systems proved not ready at the beginning of the campaign, yet were crucial to its objectives, and GVT instrumentation problems cost time which could have been put to better use.

The AFS wideband actuators and electronics are designed to interact with the aeroelastic dynamics of the aircraft in flight. However, this complicates the analysis of noise perturbations during the GVT of the aircraft. In the case of the FliPASED GVT, these systems produced a noticeable amount of electromagnetic noise, which was first associated to an instrumentation problem. After checking the GVT instrumentation and due to interferences in the modal identification results, the only solution that remained was to cut the power to the aileron actuators dedicated to the AFS control system. Given the remaining torque at rest, compared to the inertia of the ailerons, this allowed to move on with the GVT. However, this prevented the investigation of structural and AFS coupling for the greater part of the GVT.

A further analysis of this problem was eventually performed on the P-FLEX aircraft at the end of the GVT campaign. Several effects were evaluated : sensor cabling modification, sensor replacement, sensor connection, sensor separation from the structure. None of these effects showed any relevant influence on the large noise level observed. Finally, a full power-up sequence of the Direct Drives was recorded with the following sequence

1. $t = 0\,\mathrm{s}$ Start recording of the GVT channels, as for a standard GVT measurement
2. $t = 10\,\mathrm{s}$ Start power-up sequence of the Direct Drive controllers and actuators
3. $t = 28\,\mathrm{s}$ A noise coming from the Direct Drive actuators was noticeable
4. $t = 43\,\mathrm{s}$ Power-down the Direct Drive controllers and actuators
5. $t = 62\,\mathrm{s}$ Stop recording

The accelerometer signals recorded during that test are plotted in figure 15. There is an obvious and drastic increase in noise levels, starting from $t = 43\,\mathrm{s}$ coincident with the noise noticed coming from the actuators. This noise can definitely be attributed to electromagnetic pulses emitted by the Direct Drive controller or actuator, as no shaker excitation is performed during this measurement run. Though all sensors showed a specific noise pattern at the power-up of the direct drives, the light triaxial sensors were the most sensitive to this phenomenon, as depicted in figure 15c. On the contrary, the bigger ones, were less affected, see figure 15a. As the

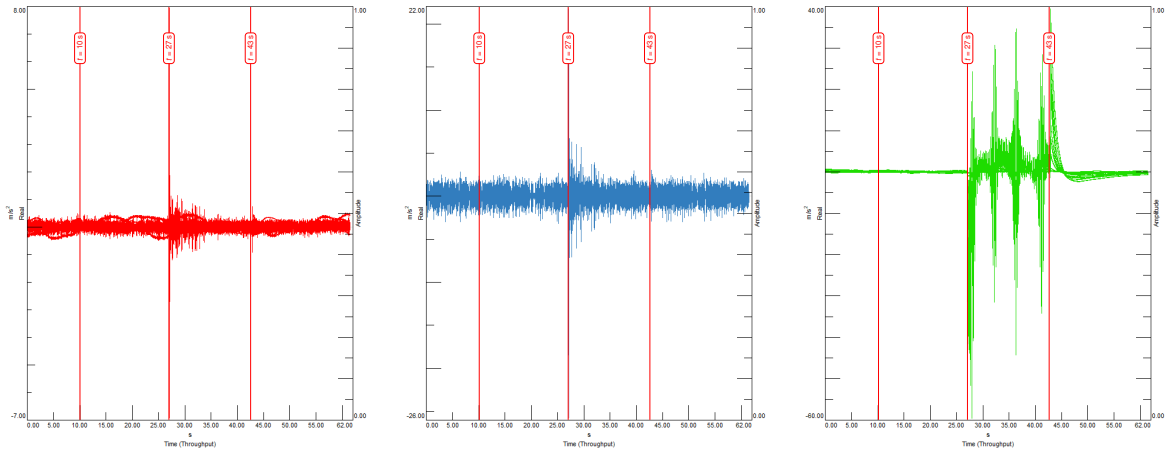

(a) Standard triaxial sensors. (b) Light uniaxial sensors. (c) Light triaxial sensors.

Figure 15: Time signals of aircraft accelerometers during the power-up test of the Direct Drives. Time key points (|).

global sensitivity comes from the combination of multiple parameters – EM exposure, distance to power supply, shielding — no component of the actuation chain could be clearly identified as the main source of the EM noise.

In order to assess the presence of noise during the test of such aircraft, a preliminary step of recordings during the power-up of the aircraft systems should be performed systematically, to determine a noise picture and potentially isolate a problematic aircraft system. Such tests are performed on industrial aircraft, but it must be reminded that the P-FLEX aircraft is a research experimental prototype.

## 5 CONCLUSION

This GVT campaign reached its main objective : characterizing the structural dynamic behaviour of the P-FLEX aircraft. An analysis was carried out in the main configuration of interest, the flutter–prone configuration, as well as two secondary configurations designed to be flutter–free. This campaign allowed to characterize the efficiency of the flutter stopper design to act on the dynamic properties of the aircraft. Although 3 structural configurations and 5 excitation points were explored during this campaign, some behaviour could not be investigated extensively or with great care, and due to the prototype nature of this aircraft, several technical and operational difficulties were encountered. Regardless, the modal models obtained during the GVT could then be used to perform flutter evaluations and update the control laws of the aircraft.

The subsequent flutter flight tests achieved the objective of the project to demonstrate the AFS functionality, at the precise flight speed forecasted by the updated models based on the GVT data, showing once more the use of such tests. It must however be highlighted that more and more active aircraft, even UAVs such as the P-FLEX, require a more thorough approach to GVT as system and structural dynamic behaviour interact with each other. While GVTs often happen late in projects, exchanges with systems and control teams should be encouraged from the early stages of such project to make the best of the short available time during GVT campaigns.

Given the different projects that explore similar UAVs for aeroelastic research, the authors hope that the findings of this paper will provide insight to some difficulties that can be met on such aircraft.

## 6 ACKNOWLEDGEMENTS

The research leading to these results is part of the FliPASED project. This project has received funding from the European Unions Horizon 2020 research and innovation program under grant agreement No. 815058.

## 7 REFERENCES

[1] *Flipased - Homepage* (2019). https://flipased.eu/index.html (visited on 01/06/2022).

[2] *FLEXOP - Homepage* (2015). https://flexop.eu/index.html (visited on 01/06/2022).

[3] *CONCERTO Project | Clean Aviation* (n.d.). https://www.concertoproject.eu (visited on 01/05/2024).

[4] *TU-Flex* (n.d.). https://www.tu.berlin/en/fmra/institutions-and-services/flight-testbeds/tu-flex (visited on 01/05/2024).

[5] Vanek, B. (2023). *Successful Demonstration of Active Flutter Suppression*. https://www.dlr.de/en/latest/news/2023/03/scientists-tame-dreaded-aviation-phenomenon (visited on 01/05/2024).

[6] Yu, F. et al. (2023). *FliPASED — Final Report*. Tech. rep. Deliverable 5.8, p. 495. https://flipased.eu/deliverables/FLIPASED_D5_8.pdf (visited on 01/05/2024).

[7] Soal, K. et al. (n.d.). Flight Vibration Testing of the T-FLEX UAV Using Online Modal Analysis. *AIAA SCITECH 2023 Forum*. American Institute of Aeronautics and Astronautics. DOI: 10.2514/6.2023-0373. https://arc.aiaa.org/doi/abs/10.2514/6.2023-0373 (visited on 28/05/2024).

[8] Sodja, J. et al. (2020). Ground Testing of the FLEXOP Demonstrator Aircraft. *AIAA Scitech 2020 Forum*. AIAA SciTech Forum. American Institute of Aeronautics and Astronautics. DOI: 10.2514/6.2020-1968. https://arc.aiaa.org/doi/10.2514/6.2020-1968 (visited on 21/05/2024).

[9] *IRIG-B Website* (n.d.). http://www.irigb.com/IRIGB_standard.html (visited on 02/05/2024).

[10] Peeters, B. et al. (2004). A New Procedure for Modal Parameter Estimation. *Sound and Vibration*.

[11] Govers, Y. et al. (2014). AIRBUS A350XWB Ground Vibration Testing: Efficient Techniques for Customer Oriented on-Site Modal Identification.

[12] Albano, E. and Rodden, W. P. (1969). A Doublet-Lattice Method for Calculating Lift Distributions on Oscillating Surfaces in Subsonic Flows. *AIAA Journal* 7.2, 279–285. ISSN: 0001-1452. DOI: 10.2514/3.5086. https://arc.aiaa.org/doi/10.2514/3.5086 (visited on 14/03/2022).

[13] Hassig, H. J. (1971). An Approximate True Damping Solution of the Flutter Equation by Determinant Iteration. *Journal of Aircraft* 8.11, 885–889. ISSN: 0021-8669. DOI: 10.2514/3.44311. https://arc.aiaa.org/doi/10.2514/3.44311 (visited on 01/05/2024).

[14] Kier, T. et al. (n.d.). Aeroservoelastic Models for Design, Testing, Flight Test Clearance and Validation of Active Flutter Suppression Control Laws. *International Forum on Aeroelasticity and Structural Dynamics IFASD 2024*. The Hague, The Netherlands.

[15] Kier, T. M. (n.d.). Comparing Different Potential Flow Methods for Unsteady Aerodynamic Modelling of a Flutter Demonstrator Aircraft. *AIAA SCITECH 2023 Forum*. American Institute of Aeronautics and Astronautics. DOI: 10.2514/6.2023-0177. https://arc.aiaa.org/doi/abs/10.2514/6.2023-0177 (visited on 23/05/2024).

## COPYRIGHT STATEMENT